Journal of Alloys and Compounds 638 (2015) 374–379

Contents lists available at ScienceDirect

Journal of Alloys and Compounds

journal homepage: www.elsevier.com/locate/jalcom

Ozone and nitrogen dioxide gas sensor based on a nanostructured $SrTi_{0.85}Fe_{0.15}O_3$ thin film

Luís F. da Silva [a,b,*], Valmor R. Mastelaro [c], Ariadne C. Catto [c], Carlos A. Escanhoela Jr. [c], Sandrine Bernardini [b], Sérgio C. Zílio [c], Elson Longo [a], Khalifa Aguir [b]

[a] LIEC, Instituto de Química, Universidade Estadual Paulista, P.O. Box 355, 14800-900 Araraquara, SP, Brazil
[b] Aix Marseille Université, CNRS IM2NP (UMR 7334), FS St Jérôme S152, Marseille 13397, France
[c] Instituto de Física de São Carlos, Universidade de São Paulo, Avenida Trabalhador São-carlense, 400, 13566-590 São Carlos, SP, Brazil

ARTICLE INFO

Article history:
Received 26 November 2014
Received in revised form 4 March 2015
Accepted 10 March 2015
Available online 19 March 2015

Keywords:
$SrTi_{1-x}Fe_xO_3$
Nanostructures
Thin films
Gas sensor
Ozone
Nitrogen dioxide

ABSTRACT

In this manuscript, we report an investigation into the sensitivity of two oxidizing gases (ozone and nitrogen dioxide) for nanocrystalline $SrTi_{0.85}Fe_{0.15}O_3$ thin films deposited by the electron beam physical vapor deposition technique. Annealing treatment at 500 °C enhanced the crystallization and surface roughness of the thin film. Electrical measurements revealed that the thin film was sensitive to oxidizing gases, especially to low ozone gas levels, exhibiting a fast response time, a short recovery time as well as good reproducibility and reversibility. These findings demonstrate the great potential of the $SrTi_{0.85}Fe_{0.15}O_3$ compound to be applied as a selective ozone gas sensor.

1. Introduction

Since the development of first gas detection device based on semiconducting metal oxides, much effort has been devoted to enhancing gas sensor performance [1–5]. Nanostructured materials have drawn the interest of many researchers due to the possibility of improving the sensitivity, selectivity, response and recovery time, as well as reducing the operating sensor temperature [2–4,6,7]. These sensors have been widely employed in industry, agriculture and in environment control to detect reducing and oxidizing gases, such as hydrocarbons, oxygen, hydrogen (H_2), nitrogen oxides (NO_2 and NO_x), ammonia (NH_3), sulfur dioxide (SO_2), carbon monoxide (CO) and ozone (O_3) [3,8–12]. Ozone (O_3) is an oxidizing gas used in important fields such as the food industry, drinking water treatment, medicine and agriculture [13–16]. Despite these important applications, ozone levels above 120 ppb become dangerous to human health, and could cause serious health problems [13,17]. Therefore, the continuous monitoring of ozone levels present in the atmosphere is indispensable. Typical ozone gas sensors are based on SnO_2, ZnO, WO_3 and In_2O_3 compounds [7,9,11,12,18–22]. Despite the progress made, numerous studies have focused on enhancing gas sensing properties, especially selectivity [23–26].

Strontium titanate ferrite ($SrTi_{1-x}Fe_xO_3$, abbreviated STFO) solid solutions are p-type semiconductors which exhibit a cubic perovskite-like structure [12,27,28]. The replacement of Ti^{4+} by Fe^{3+} creates negatively charged defects (Fe'_{Ti}) [27–31], which due to the electroneutrality conditions, are compensated by the formation of oxygen vacancies (Vö) [28,32]. These solid solutions have been applied as resistive gas sensors, mainly for oxygen and hydrocarbons [1,10,12,31,33–37]. As shown in Table 1, different methodologies have been employed to prepare STFO thick and/or thin films.

In recent years, our group has dedicated efforts toward investigating STFO ($0.0 \leqslant x \leqslant 1.0$) solid solutions prepared by using different synthesis routes [7,38–40]. In an earlier study, the long- and short-range order structure and electronic properties of nanostructured STFO powders were studied [7]. Additionally, for the first

* Corresponding author at: LIEC, Instituto de Química, Universidade Estadual Paulista, P.O. Box 355, 14800-900 Araraquara, SP, Brazil. Tel.: +55 16 33016643.
E-mail addresses: lfsilva83@gmail.com (L.F. da Silva), khalifa.aguir@im2np.fr (K. Aguir).

http://dx.doi.org/10.1016/j.jallcom.2015.03.089
0925-8388/

Table 1
Brief summary of results reported for $SrTi_{1-x}Fe_xO_3$ compounds prepared by various methodologies applied as resistive gas sensors toward various target gases.

Preparation methodology	Composition	Operating temp. (°C)	Target gas	References
Mixed oxides reaction	$SrTi_{0.60}Fe_{0.40}O_3$; $SrTi_{0.40}Fe_{0.60}O_3$	700	O_2, NO, NO_2, CO, CO_2,CH_4	[36]
Mixed oxides reaction	$SrTi_{0.65}Fe_{0.35}O_3$:La	>600	SO_2	[34]
Pulsed laser deposition	$SrTi_{0.65}Fe_{0.35}O_3$	~500 °C	O_2	[12]
Mixed oxides reaction	$SrTi_{0.60}Fe_{0.40}O_3$	350	C_3H_8	[8]
Self-propagating high-temperature reaction	$SrTi_{0.40}Fe_{0.60}O_3$	650	O_2	[10]
Electrospinning	$SrTi_{0.65}Fe_{0.35}O_3$	750	O_2	[35]
Aerosol	$SrTi_{0.70}Fe_{0.30}O_3$	400	O_2, C_3H_8	[6]
Sol–gel	$SrTi_{0.50}Fe_{0.50}O_3$	>450	O_2	[37]

time, the ozone gas sensing properties of nanostructured STFO thin films deposited by electron-beam physical vapor deposition (EB–PVD) were also studied, looking at the influence of the Fe content on ozone gas sensing films [39]. Despite continued progress, the gas sensing properties, particularly the sensitivity of STFO toward ozone and other analyte gases, requires further investigation.

In this study, we present a detailed investigation of O_3 and NO_2 sensing properties of nanostructured $SrTi_{0.85}Fe_{0.15}O_3$ (abbreviated as STFO15) thin films deposited by the electron beam physical vapor deposition (EB–PVD) method. The structural and microstructural properties of STFO15 samples were characterized by X-ray absorption spectroscopy (XAS) and atomic force microscopy analysis, respectively. Gas sensing properties of STFO15 thin film samples toward O_3, NO_2, NH_3, and CO gases were evaluated, mainly concerning its selectivity. Therefore, the focus of this research was to provide a better understanding about the gas sensing properties of the nanostructured $SrTi_{1-x}Fe_xO_3$ compound.

2. Experimental section

2.1. Deposition of $SrTi_{0.85}Fe_{0.15}O_3$ thin film and characterization techniques

The electron beam deposition technique was used for STFO15 thin film deposition. A target was produced from a nanocrystalline $SrTi_{0.85}Fe_{0.15}O_3$ powder sample synthesized via the polymeric precursor method [40]. The STFO15 thin film, the thickness of which was monitored by a quartz balance, was deposited in a Balzers BAK600 evaporator on Si(100) and SiO_2/Si substrates containing 120 nm-thick Pt electrodes. After deposition, the thin films were annealed in an electric furnace under an air atmosphere for 4 h at 500 °C with a heating rate of 5 °C min^{-1} [39]. Additional details regarding the synthesis procedure of the target as well as the thin film deposition can be found in Refs. 27,40.

The thin film surface microstructural characteristics were investigated using an atomic force microscope (NT-MDT SolverPro AFM) in tapping mode. The sample thickness was verified by using a field emission scanning electron microscope (FE-SEM, Zeiss Supra35) operating at 5 kV. The microanalysis by energy-dispersive X-ray (EDX) spectroscopy was performed in a spectrometer EDAX-AMETEC (model APPOLLO X).

X-ray absorption spectroscopy (XAS) experiments were carried at the Brazilian Synchrotron Light Laboratory (LNLS), using the XAFS2 beamline. This characterization technique was applied to probe the medium- and short-range order structure of STFO15 thin films deposited onto Si(100) before and after thermal treatment. Ti K-edge XANES (X-ray absorption near-edge spectroscopy) spectra were collected in fluorescence mode, at room temperature, using a 15-element Ge solid state detector (Ge-15). These spectra were recorded between 4960 and 5060 eV using an energy step of 0.3 eV around the edge. For comparison purposes among the different samples, all spectra were background removed and normalized using the first EXAFS oscillation as unity.

2.2. Gas-sensing measurements

The sensing properties of nanocrystalline STFO15 film toward ozone (O_3), nitrogen dioxide (NO_2), carbon monoxide (CO) and ammonia (NH_3) gases were evaluated. The thin film was inserted into a special chamber which allowed for the control of the temperature and target gas concentrations. The sensor operating temperature ($T_{opt.}$), which varied from 220 °C to 300 °C, was maintained by an external heating source based on an Hg lamp driven by a regulated power supply. A 1 V *dc* voltage was applied to the thin film while the electrical resistance was monitored using an electrometer (HP4140B Source/Pico-ammeter). Dry air was used as both the reference and the carrier gas for all gases, maintaining a constant total flow of 8.3 cm^3 s^{-1} via mass flow controllers. Ozone gas was generated by oxidizing oxygen using a pen-ray UV lamp (UVP company, model 97-0067-01), which was calibrated given an O_3 level range between 0.1 and 0.8 ppm. NO_2 gas sensing measurements were performed under concentrations varying from 5 to 40 ppm. CO and NH_3 gases were also employed in the range of 5–40 ppm. A schematic illustration of the STFO15 film based gas sensor, and a photograph of the chamber used for gas-sensing experiments are presented in Fig. 1.

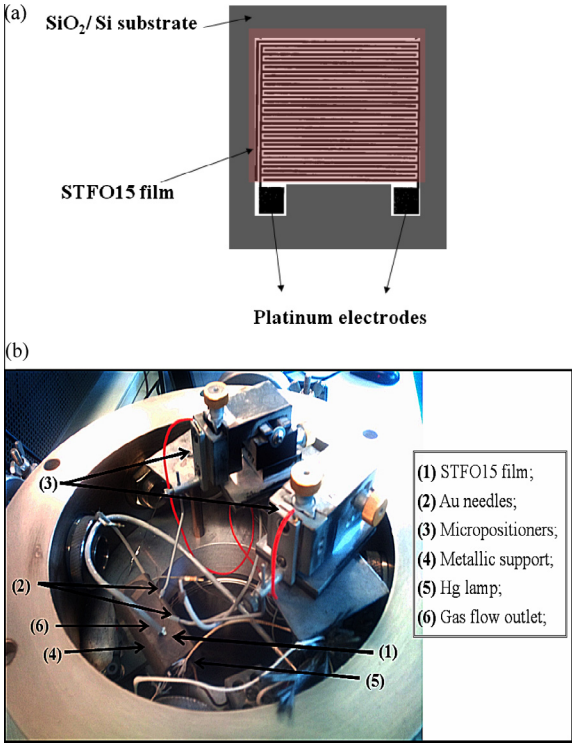

Fig. 1. Preparation and gas-sensing tests of the gas sensor device. (a) Schematic structure of the sensor device. (b) Photograph of the gas sensor test chamber.

The gas response or sensitivity (S) was defined as $S = R_{air}/R_{gas}$, where R_{air} and R_{gas} are the electric resistances of the sensor device exposed to dry air and oxidizing gases (O_3 or NO_2), respectively.

3. Results and discussion

3.1. Structural and microstructural characterizations

Fig. 2 displays the Ti-K edge XANES spectra of the STFO15 thin film before and after thermal treatment at 500 °C for 4 h. Three transitions labeled as P1, P2, and P3 are denoted on the pre-edge region of XANES spectra. Peak P1 is related to the $1s(Ti) \rightarrow 3d(t_{2g})(Ti)$ transition, whereas P2 peak is due to the $1s(Ti) \rightarrow 4p(Ti)$ transition, including some degree of the

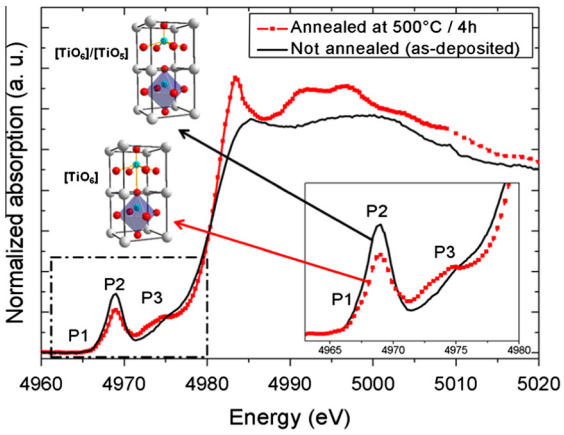

Fig. 2. Ti-K edge spectra of STFO15 thin film before and after annealing at 500 °C for 4 h. The inset shows the pre-edge region of XANES spectra.

1s(Ti) → 3d(e_g)(Ti) quadrupole contribution [7,28]. The P3 peak is assigned to a dipole excitation of 1s electrons to t_{2g} and e_g orbitals of the neighboring TiO_6 [28,41].

Previous results have shown that P2 intensity is directly related to Ti symmetry, exhibiting the lowest intensity for the crystalline cubic structure, whereas in non-crystalline structures it becomes more intense [41]. In amorphous titanate compounds, the intense P2 peak was attributed to the presence of (TiO_6) and (TiO_5) units [42–45].

Fig. 2 inset shows a lower intensity of the P2 peak after annealing treatment, which can be attributed to an increase in (TiO_6) units. Additionally, the P3 peak was visible in the spectrum of annealed sample, revealing an increase in TiO_6 octahedra linkage. Likewise, the oscillations in the post-edge region (4980–5020 eV) were more pronounced after annealing. These three effects caused by annealing can be interpreted as an increase in the short and medium range-order around titanium atoms, allowing for the conclusion that the degree of crystallization of the STFO15 sample increased after annealing.

Fig. 3 shows the AFM images of the STFO15 thin film before and after annealing at 500 °C. Before annealing, the sample exhibited a flat surface with an R_{rms} (root-mean-square) roughness around 0.748 nm. After annealing, the sample presented a microstructure characteristic of nanocrystalline thin films exhibiting grain sizes between 30 and 150 nm and an R_{rms} around 4.0 nm.

Fig. 4 shows the EDX spectra of the STFO15 ceramic pellet (used as target) and STFO15 thin film after annealing treatment. The EDX spectra detected the presence of Sr, Ti, Fe, and O elements in both samples, whereas the Si peak was observed only for the thin film. Additionally, the (Sr + Ti)/Fe ratio was approximately 1.2 (ceramic pellet) and 1.4 (thin film), suggesting that the stoichiometry of the STFO15 thin film was preserved during the deposition process (see Fig. 4).

3.2. Gas sensing properties

First, the electrical resistance of the STFO15 thin film before annealing exhibited a higher resistivity, due the presence of several porous (see Fig. 3), resulting in a low densification of the sample. The electrical resistance of the STFO15 thin film annealed at 500 °C presented typical values of metal oxide semiconductor sensors and was then monitored when exposed to 0.8 ppm of O_3 (Fig. 5a) and 40 ppm of NO_2 (Fig. 5b) for various periods of time at an operating temperature of 260 °C for O_3 and 220 °C for NO_2. As can be seen, the gas sensor response of the STFO15 thin film was characteristic of a p-type semiconductor [4]. In addition, the STFO15 thin film showed good sensitivity, even for short periods of time, total reversibility and good stability of the baseline toward O_3 and NO_2 gases. For NO_2 gas, it was observed that the sample reached a saturation level at times longer than 30 s.

It is well-established that the detection of oxidizing gases on a p-type sensor material is based on the surface adsorption of the gas

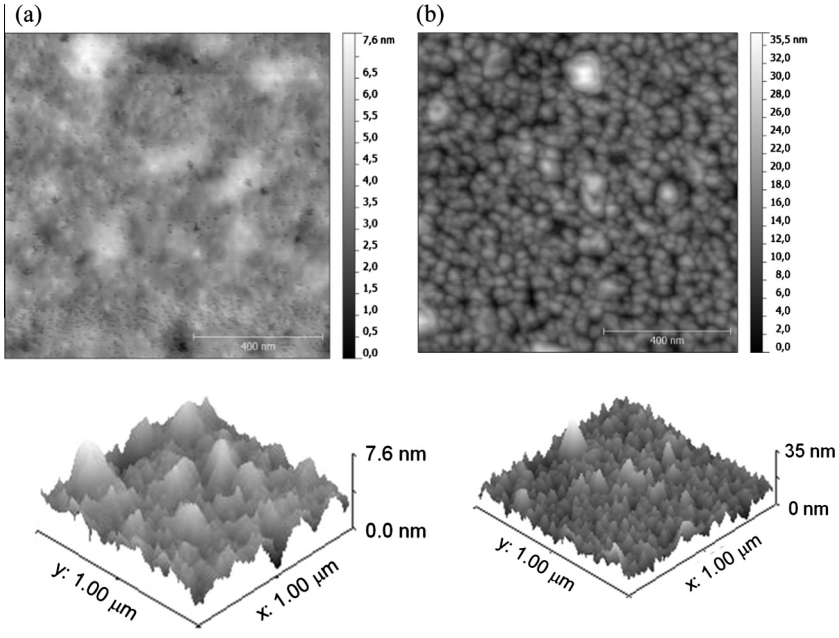

Fig. 3. AFM images of STFO15 thin film (a) before and (b) after annealing treatment at 500 °C for 4 h.

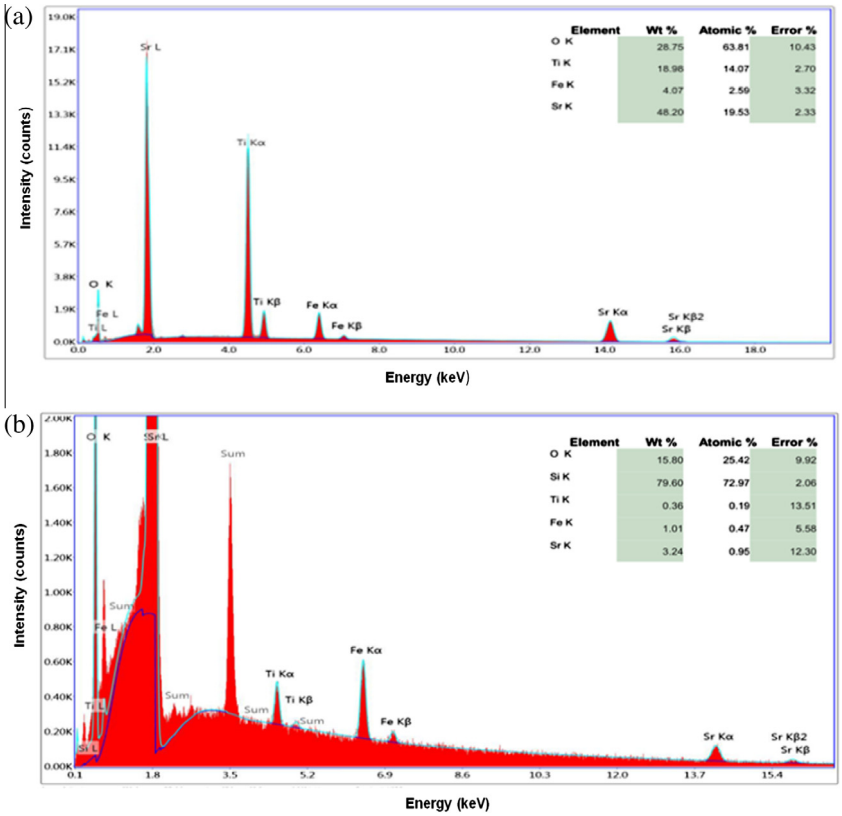

Fig. 4. Energy dispersive X-ray (EDX) spectroscopy analysis of the (a) STFO15 ceramic pellet and (b) STFO15 thin film annealing treated at 500 °C.

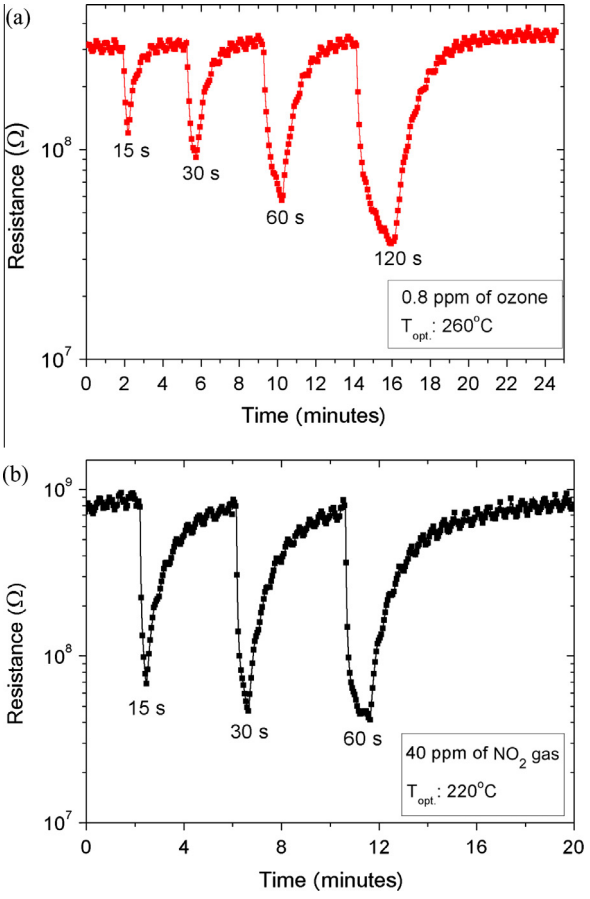

Fig. 5. Gas sensing response of the STFO15 thin film exposed for different times: (a) 0.8 ppm O_3 at 260 °C and (b) 40 ppm NO_2 at 220 °C.

molecules, leading to the formation of a hole-accumulation layer which causes an increase in the current density [4,46,47]. The gas sensor response of the STFO15 thin film for these two oxidizing gases (O_3 and NO_2) can be explained by the follow reactions [18,46]:

$$O_{3(g)} + e^- \rightarrow O_{2(des)} + O^-_{(ads)} \quad (1)$$

$$NO_{2(g)} + e^- \rightarrow NO^-_{2(ads)} \quad (2)$$

$$NO^-_{2(ads)} + O^-_{(ads)} + 2e^- \rightarrow NO_{(ads)} + O^-_{(ads)} \quad (3)$$

To determine the optimum operating temperature ($T_{opt.}$), the annealed STFO15 thin film was exposed for 30 s–0.8 ppm of O_3 and afterward to 40 ppm of NO_2. The results presented in Fig. 6 show a maximum sensitivity value at 260 °C for both target gases, which is close to that of traditional metal oxide gas sensors such as WO_3, In_2O_3, and SnO_2 [9,11,12,19,20,46,48]. Chow and co-workers synthesized STFO thin films via a sol–gel spin-coating method and applied them as oxygen gas sensors, with an operating temperature ranging around of 350 °C for an iron content of $x = 0.2$ [49]. On the other hand, STFO thick films obtained via solid-state reaction method exhibited good gas sensing performance toward oxygen at temperatures above 600 °C [33,34,36,50].

Based on the above results, the STFO15 thin film was kept at 260 °C and then exposed for 30 s to different O_3 levels (0.1–0.8 ppm). As can be seen in Fig. 7, it is noteworthy that the film displayed good sensitivity even at lower O_3 levels, total reversibility, as well as good reproducibility. In addition, the response time varied from 26 s (0.1 ppm) to 28 s (0.8 ppm), while the recovery time varied from 72 s (0.1 ppm) to 161 s (0.8 ppm). Although the response time (t_{res}) for STFO15 thin film was greater than for WO_3 compound ($t_{res} \sim 1$ s), the recovery time (t_{rec}) was relatively shorter ($t_{rec} < 60$ s) [11].

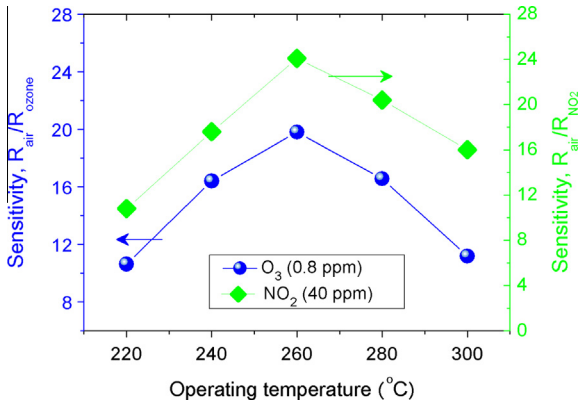

Fig. 6. Gas sensor response of the STFO15 thin film exposed to 0.8 ppm O_3 and 40 ppm NO_2 at different operating temperatures.

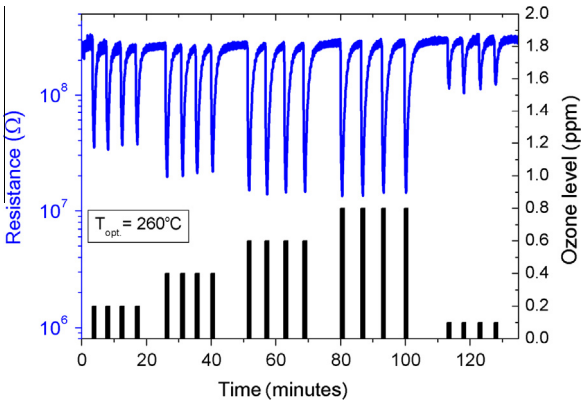

Fig. 7. Ozone gas sensing response for the STFO15 thin film as a function of the gas level at an operating temperature of 260 °C.

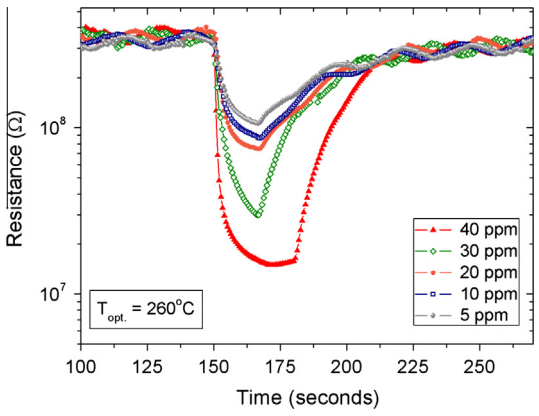

Fig. 8. NO_2 gas sensing responses for STFO15 thin film at 260 °C for various NO_2 levels (5–40 ppm).

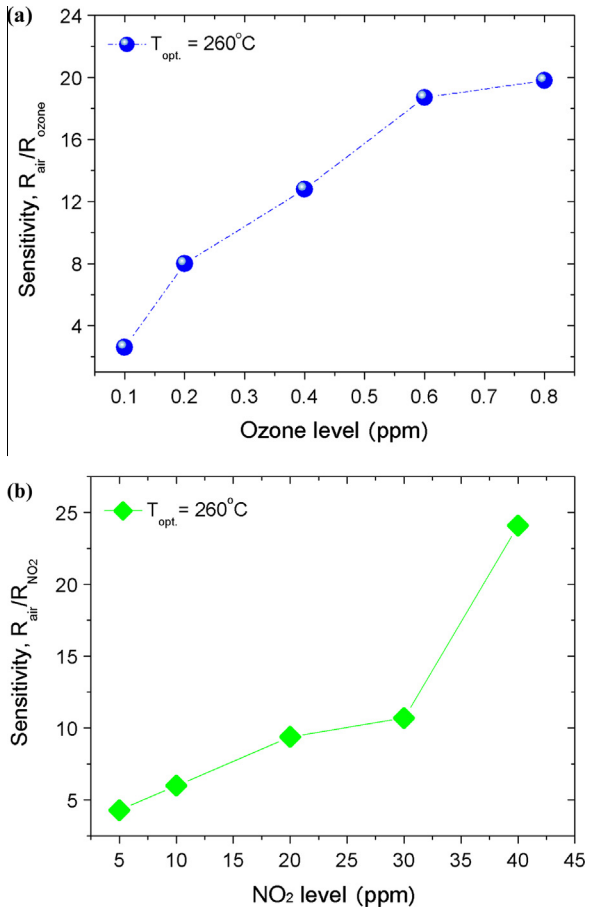

Fig. 9. Sensitivity versus gas concentration in the range (a) 0.1–0.8 ppm O_3 and (b) 5–40 ppm NO_2.

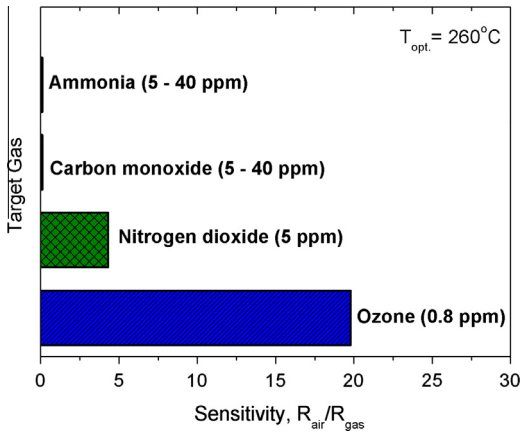

Fig. 10. Gas sensor response of the STFO15 thin film to oxidizing (O_3 and NO_2) and reducing (CO and NH_3) gases at an operating temperature of 260 °C.

In a similar procedure, the annealed STFO15 thin film was also kept at 260 °C and exposed to NO_2 gas. As depicted in Fig. 8, even at 5 ppm NO_2, the material showed a noticeable response as well as good reproducibility and reversibility.

Gas sensing experiments were also performed using the carbon monoxide (CO) and ammonia (NH_3) gases. The STFO15 thin film did not exhibit any sensitivity to these gases in the range of 5 to 40 ppm when measured at different operating temperatures (220–300 °C).

Fig. 9(a) and (b) shows the sensitivity values of the annealed STFO15 thin film as function of O_3 and NO_2 concentrations, respectively, at a working temperature of 260 °C. In the case of O_3 gas, the sensitivity increased with the gas concentration, reaching a saturation level above 0.6 ppm, whereas for NO_2 gas, the saturation level was not reached even at the highest concentration allowed by the mass flux controller.

Gas selectivity is one of the most important parameters and also a challenge for the manufacture of metal-oxide gas sensor

devices [2,4,51]. Fig. 10 displays the comparison of the sensitivity values of the annealed STFO15 thin film when exposed to oxidizing (O_3 and NO_2) and reducing (CO and NH_3) gases at 260 °C. In order to further exploit the selectivity of the film, we chose similar gas concentrations, i.e., 0.8 ppm O_3 and 5 ppm NO_2, to compare the gas sensing performance. As can be seen, the annealed STFO15 thin film showed the highest sensitivity to O_3 (19.8) when compared to NO_2 (4.3) and non-detectable sensitivity to CO and NH_3 gases. Based on these findings, we can state that the STFO15 thin film can be considered as a promising material for an ozone gas sensor.

4. Conclusions

We have successfully obtained nanocrystalline $SrTi_{0.85}Fe_{0.15}O_3$ thin films via the electron beam deposition technique. X-ray absorption spectroscopy measurements showed that the annealing treatment was effective in increasing the degree of crystallization of the STFO15 thin film, which led to an increase in surface roughness, according to AFM analysis.

Electrical resistance measurements pointed out the good sensitivity, fast response and short recovery time of the annealed STFO15 thin film when exposed to O_3 and NO_2 oxidizing gases. Due to the good sensing properties to ozone gas, this material can be considered as a promising material for ozone gas sensors.

Acknowledgments

The authors are grateful for the financial support from the Brazilian research funding institution CNPq (MCT/CNPq, under Grants Nos. 70/2008 and 150753/2013-6) and FAPESP (under Grants Nos. 2013/09573-3, 2013/07296-2, 2013/12473-0 and 2012/15170-6). This research was partially performed at the Brazilian Laboratory of Synchrotron Radiation (LNLS) and the Brazilian Nanotechnology National Laboratory (LNNano), Microfabrication laboratory (Project 17168), Campinas, SP, Brazil.

References

[1] A. Rothschild, H.L. Tuller, J. Electroceram. 17 (2006) 1005–1012.
[2] G. Jimenez-Cadena, J. Riu, F.X. Rius, Analyst 132 (2007) 1083–1099.
[3] G. Korotcenkov, Handbook of Gas Sensor Materials: Properties, Advantages and Shortcomings for Applications, Springer, New York, 2013.
[4] H.-J. Kim, J.-H. Lee, Sens. Actuators, B 192 (2014) 607–627.
[5] L.F. da Silva, A.C. Catto, W. Avansi, L.S. Cavalcante, J. Andres, K. Aguir, V.R. Mastelaro, E. Longo, Nanoscale 6 (2014) 4058–4062.
[6] K. Sahner, M. Kaspar, R. Moos, Sens. Actuators, B 139 (2009) 394–399.
[7] A.C. Catto, L.F. da Silva, M.I.B. Bernardi, M.S. Li, E. Longo, P.N. Lisboa-Filho, O.R. Nascimento, V.R. Mastelaro, J. Nanopart. Res. 16 (2014) 1–9.
[8] P. Meuffels, J. Eur. Ceram. Soc. 27 (2007) 285–290.
[9] K. Aguir, C. Lemire, D.B.B. Lollman, Sens. Actuators, B 84 (2002) 1–5.
[10] G. Neri, G. Micali, A. Bonavita, R. Licheri, R. Orrù, G. Cao, D. Marzorati, E. Merlone Borla, E. Roncari, A. Sanson, Sens. Actuators, B 134 (2008) 647–653.
[11] M. Bendahan, R. Boulmani, J.L. Seguin, K. Aguir, Sens. Actuators, B 100 (2004) 320–324.
[12] S.J. Litzelman, A. Rothschild, H.L. Tuller, Sens. Actuators, B 108 (2005) 231–237.
[13] L.C. Simoes, M. Simoes, RSC Adv. 3 (2013) 2520–2533.
[14] S. Patil, P. Bourke, J.M. Frias, B.K. Tiwari, P.J. Cullen, Innov. Food Sci. Emerg. Technol. 10 (2009) 551–557.
[15] H.-P. Kaiser, O. Koester, M. Gresch, P.M.J. Perisset, P. Jaeggi, E. Salhi, et al., Ozone: Sci. Eng. 35 (2013) 168–185.
[16] L.S. Hansen, P. Hansen, K.M.V. Jensen, J. Stored Prod. Res. 54 (2013) 59–63.
[17] C.Y. Wang, R.W. Becker, T. Passow, W. Pletschen, K. Köhler, V. Cimalla, O. Ambacher, Sens. Actuators, B 152 (2011) 235–240.
[18] M. Acuautla, S. Bernardini, L. Gallais, T. Fiorido, L. Patout, M. Bendahan, Sens. Actuators, B 203 (2014) 602–611.
[19] A.C. Catto, L.F. da Silva, C. Ribeiro, S. Bernardini, K. Aguir, E. Longo, V.R. Mastelaro, RSC Adv. 5 (2015) 19528–19533.
[20] G. Korotcenkov, B.K. Cho, Sens. Actuators, B 161 (2012) 28–44.
[21] D. Barreca, D. Bekermann, E. Comini, A. Devi, R.A. Fischer, A. Gasparotto, C. Maccato, C. Sada, G. Sberveglieri, E. Tondello, CrystEngComm 12 (2010) 3419–3421.
[22] A. Gurlo, Nanoscale 3 (2011) 154–165.
[23] T. Xiao, X.Y. Wang, Z.H. Zhao, L. Li, L. Zhang, H.C. Yao, J.S. Wang, Z.J. Li, Sens. Actuators, B 199 (2014) 210–219.
[24] Q. Simon, D. Barreca, A. Gasparotto, C. Maccato, E. Tondello, C. Sada, E. Comini, A. Devi, R.A. Fischer, Nanotechnology 23 (2012) 025502.
[25] A. Sharma, M. Tomar, V. Gupta, Sens. Actuators, B 181 (2013) 735–742.
[26] X.T. Yin, X.M. Guo, Sens. Actuators, B 200 (2014) 213–218.
[27] L.F. da Silva, J.-C. M'Peko, J. Andrés, A. Beltrán, L. Gracia, M.I.B. Bernardi, A. Mesquita, E. Antonelli, M.L. Moreira, V.R. Mastelaro, J. Phys. Chem. C 118 (2014) 4930–4940.
[28] M. Vračar, A. Kuzmin, R. Merkle, J. Purans, E.A. Kotomin, J. Maier, O. Mathon, Phys. Rev. B 76 (2007) 174107.
[29] A. Rothschild, W. Menesklou, H.L. Tuller, E. Ivers-Tiffee, Chem. Mater. 18 (2006) 3651–3659.
[30] E. Blokhin, E. Kotomin, A. Kuzmin, J. Purans, R. Evarestov, J. Maier, Appl. Phys. Lett. 102 (2013) 112913.
[31] A. Rothschild, S.J. Litzelman, H.L. Tuller, W. Menesklou, T. Schneider, E. Ivers-Tiffée, Sens. Actuators, B 108 (2005) 223–230.
[32] L.H. Brixner, Mater. Res. Bull. 3 (1968) 299–308.
[33] G. Neri, A. Bonavita, G. Micali, G. Rizzo, R. Licheri, R. Orrù, G. Cao, Sens. Actuators, B 126 (2007) 258–265.
[34] A. Sanson, E. Mercadelli, E. Roncari, R. Licheri, R. Orrù, G. Cao, E. Merlone-Borla, D. Marzorati, A. Bonavita, G. Micali, G. Neri, Ceram. Int. 36 (2010) 521–527.
[35] S.-H. Choi, S.-J. Choi, B.K. Min, W.Y. Lee, J.S. Park, I.-D. Kim, Macromol. Mater. Eng. 298 (2013) 521–527.
[36] G. Jin, G. Choi, W. Lee, J. Park, J. Nanosci. Nanotechnol. 11 (2011) 1738–1741.
[37] W. Lee, D. Na, J. Park, J. Ceram. Process. Res. 13 (2012) 717–720.
[38] L.F. da Silva, W. Avansi Jr., M.L. Moreira, J. Andres, E. Longo, V.R. Mastelaro, CrystEngComm 14 (2012) 4068–4073.
[39] V.R. Mastelaro, S.C. Zílio, L.F. da Silva, P.I. Pelissari, M.I.B. Bernardi, J. Guerin, K. Aguir, Sens. Actuators, B 181 (2013) 919–924.
[40] L.F. da Silva, M.I.B. Bernardi, L.J.Q. Maia, G.J.M. Frigo, V.R. Mastelaro, J. Therm. Anal. Calorim. 97 (2009) 173–177.
[41] R.V. Vedrinskii, V.L. Kraizman, A.A. Novakovich, P.V. Demekhin, S.V. Urazhdin, J. Phys.: Condens. Matter 10 (1998) 9561–9580.
[42] V.M. Longo, A.T. de Figueiredo, S. de Lazaro, M.F. Gurgel, M.G.S. Costa, C.O. Paiva-Santos, J.A. Varela, E. Longo, V.R. Mastelaro, F.S. deVicente, A.C. Hernandes, R.W.A. Franco, J. Appl. Phys. 104 (2008) 023515.
[43] A.T. de Figueiredo, V.M. Longo, R.O. da Silva, V.R. Mastelaro, A. Mesquita, R.W.A. Franco, J.A. Varela, E. Longo, Chem. Phys. Lett. 544 (2012) 43–48.
[44] A.T. de Figueiredo, V.M. Longo, S. de Lazaro, V.R. Mastelaro, F.S. De Vicente, A.C. Hernandes, M.S. Li, J.A. Varela, E. Longo, J. Lumin. 126 (2007) 403–407.
[45] S. de Lazaro, J. Milanez, A.T. de Figueiredo, V.M. Longo, V.R. Mastelaro, F.S. De Vicente, J.A. Varela, E. Longo, Appl. Phys. Lett. 90 (2007) 111904.
[46] S. Maeng, S.-W. Kim, D.-H. Lee, S.-E. Moon, K.-C. Kim, A. Maiti, ACS Appl. Mater. Interfaces 6 (2013) 357–363.
[47] D. Peeters, D. Barreca, G. Carraro, E. Comini, A. Gasparotto, C. Maccato, C. Sada, G. Sberveglieri, J. Phys. Chem. C 118 (2014) (1819) 11813–11819.
[48] G. Korotcenkov, V. Macsanov, V. Tolstoy, V. Brinzari, J. Schwank, G. Faglia, Sens. Actuators, B 96 (2003) 602–609.
[49] C.L. Chow, W.C. Ang, M.S. Tse, O.K. Tan, Thin Solid Films 542 (2013) 393–398.
[50] W. Menesklou, H.-J. Schreiner, K.H. Härdtl, E. Ivers-Tiffée, Sens. Actuators, B 59 (1999) 184–189.
[51] A. Gurlo, R. Riedel, Angew. Chem. Int. Ed. 46 (2007) 3826–3848.